minerals

MDPI

Supplementary Material

Phosphate Removal from Wastewater by Magnetic Amorphous Lanthanum Silicate Alginate Hydrogel Beads

Hongyun Chen [1,2], Hongbo Zeng [2,*] and Huaming Yang [1,3,4,5,*]

[1] Hunan Key Laboratory of Mineral Materials and Application, School of Minerals Processing and Bioengineering, Central South University, Changsha 410083, China; chenhongyun@csu.edu.cn
[2] Department of Chemical and Materials Engineering, University of Alberta, Edmonton, Alberta, AB T6G 1H9, Canada
[3] Engineering Research Center of Nano-Geomaterials of Ministry of Education, China University of Geosciences, Wuhan 430074, China
[4] Faculty of Materials Science and Chemistry, China University of Geosciences, Wuhan 430074, China
[5] Key Laboratory of Functional Geomaterials in China Nonmetallic Minerals Industry, China University of Geosciences, Wuhan 430074, China
* Correspondence: hongbo.zeng@ualberta.ca (H.Z.); hmyang@csu.edu.cn, hm.yang@cug.edu.cn (H.Y.); Tel.: +1-780-492-1044 (H.Z.); +86-731-88830549 (H.Y.)

Text S1 Kinetic models:

$$\ln(q_e - q_t) = \ln q_e - k_1 t \quad (1)$$

$$\frac{t}{q_t} = \frac{1}{k_2 q_e^2} + \frac{t}{q_e} \quad (2)$$

where q_e (mg/g) and q_t (mg/g) were the adsorption capacity at equilibrium and at time t, and the k_1 (min^{-1}) and k_2 ($g \cdot mg^{-1} \cdot min^{-1}$) were the adsorption rate constants of the pseudo-first-order and pseudo-second-order models, respectively.

Text S2 Adsorption isotherms models (Langmuir, Freundlich, and Langmuir-Freundlich models):

$$q_e = \frac{q_{max} K_L C_e}{1 + K_L C_e} \quad (3)$$

$$q_e = K_F C_e^{1/n} \quad (4)$$

$$q_e = \frac{q_{max} K_{LF} C_e^{n_2}}{1 + K_{LF} C_e^{n_2}} \quad (5)$$

where q_e (mg P/g) was the adsorbed amount of phosphate at equilibrium, C_e (mg P/L) was the concentration of phosphate at equilibrium, q_{max} (mg P/g) was the maximum phosphate sorption capacity, K_L (L/mg) was the Langmuir constant, and q_{max} (mg P/g) was the maximum phosphate sorption capacity. K_F (mg/g) and $1/n$ were Freundlich constants related to adsorption capacity and adsorption density. K_{LF} (L/mg) was the Langmuir-Freundlich constant and $n_2$was the index of heterogeneity.

Text S3 Equation for calculating the adsorption capacity of phosphate and removal efficiency of P:

$$q_t = \frac{V(C_0 - C_t)}{M} \quad (6)$$

$$\eta = \frac{(C_0 - C_t)}{C_0} \times 100\% \quad (7)$$

where q_t(mg/g) was the adsorption capacity at time *t*, *V*(L) represented the volume of phosphate solution, C_0 (mgP/L) and C_t (mgP/L) were the P concentrations in solution, *M*(g) was the mass of added adsorbent, and η was the removal efficiency of P, respectively.

Table S1. Adsorption kinetic parameters for phosphorus adsorption by the synthesized hydrogel beads.

Samples	Pseudo-first-order model			Pseudo-second-order model		
	k_1	q_e (mg/g)	R^2	k_2	q_e (mg/g)	R^2
MALS-B	0.200	12.283	0.927	0.015	15.092	0.963
ALS-B	0.216	18.281	0.960	0.010	22.446	0.987
MS-B	0.421	0.236	0.242	2.359	0.263	0.288

Table S2. Adsorption isotherm parameters for phosphorus adsorption by the synthesized hydrogel beads.

Samples	Langmuir			Freundlich			Langmuir-Freundlich		
	K_L	q_e(mg/g)	R^2	K_F	N	R^2	K_{LF}	q_e(mg/g)	R^2
MALS-B	0.048	50.342	0.949	5.869	2.174	0.879	0.016	40.137	0.964
ALS-B	0.078	48.608	0.972	8.622	2.581	0.908	0.067	46.077	0.969
MS-B	0.011	8.430	0.944	0.168	1.353	0.918	0.001	3.869	0.982

Table S3. The fitting parameters of O 1*s* peak of MALS-B before and after phosphate adsorption.

Samples	Peak	Position (eV)	Area	FWHM (eV)	Percentage (%)
MALS-B	M-O	530.84	108394.80	2.2	26.26
	M-OH	531.66	233587.53	1.76	56.60
	H_2O	532.53	70744.47	2.04	17.15
MALS-B after phosphate adsorption	M-O	530.79	141919.08	1.74	30.76
	M-OH	531.60	228571.95	1.52	49.55
	H_2O	532.56	90798.32	1.68	19.69

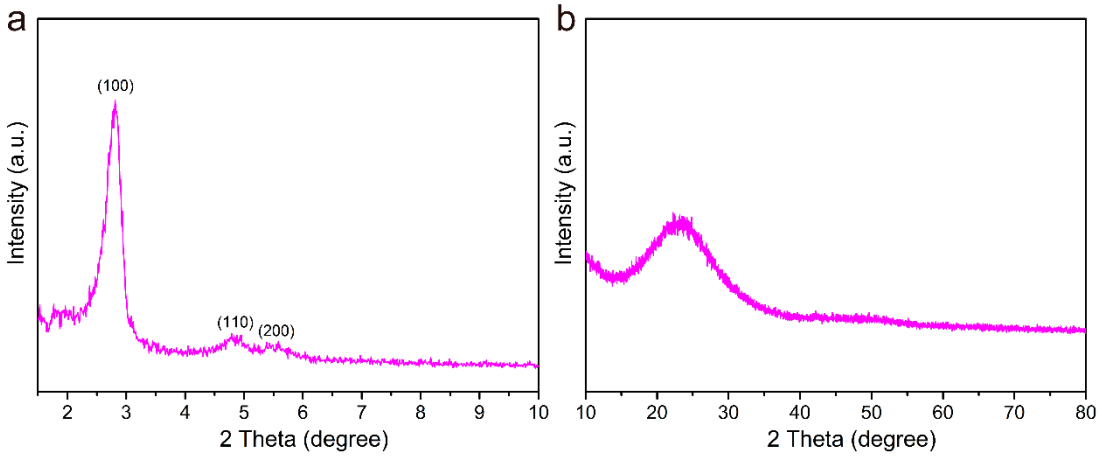

Figure S1. (**a**)SAXRD and (**b**) WAXRD patterns of mesoporous silica materials.

Figure S1 shows SAXRD and WAXRD patterns of mesoporous silica materials. The SAXRD patterns of mesoporous silica materials had obvious (100), (110), and (200) diffraction peaks corresponded to the mesoporous structure, demonstrating the highly ordered and hexagonal structure of mesoporous silica. The WAXRD patterns of mesoporous silica materials proved that mesoporous silica materials were amorphous SiO_2.

To characterize the mesopore structure, TEM images of mesoporous silica materials are presented in Figure S2. Channels of mesopores were long-range ordered in vertical channel direction and had a hexagonal structure along the channel direction.

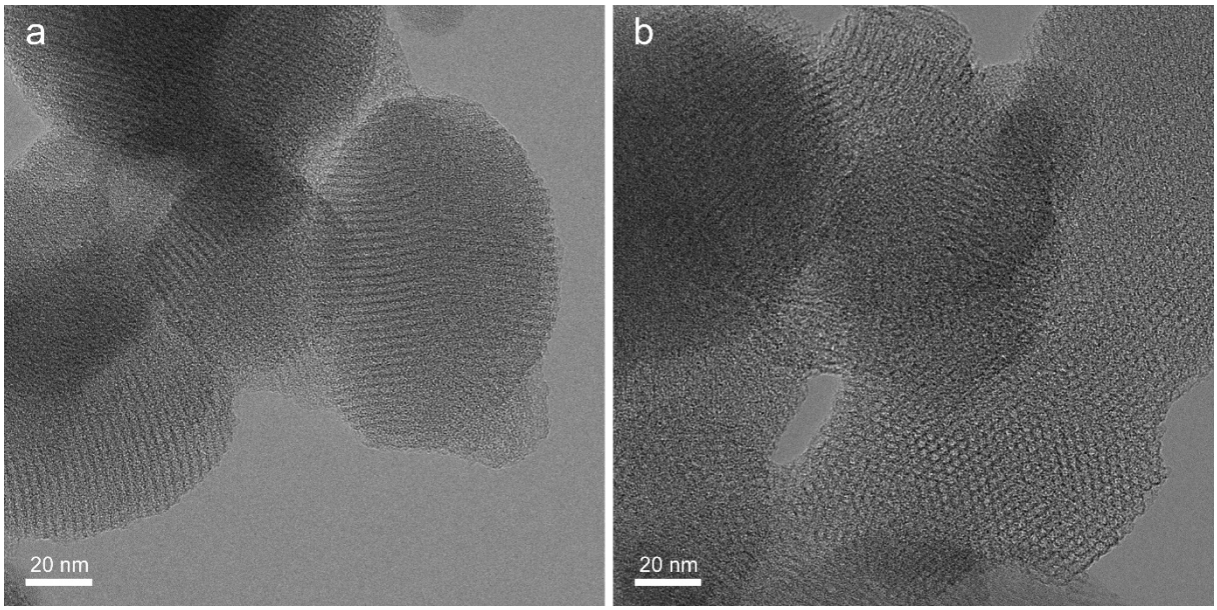

Figure S2. TEM images of mesoporous silica materials: (**a**) in the direction of the pore axis; (**b**) in the direction perpendicular to the pore axis.

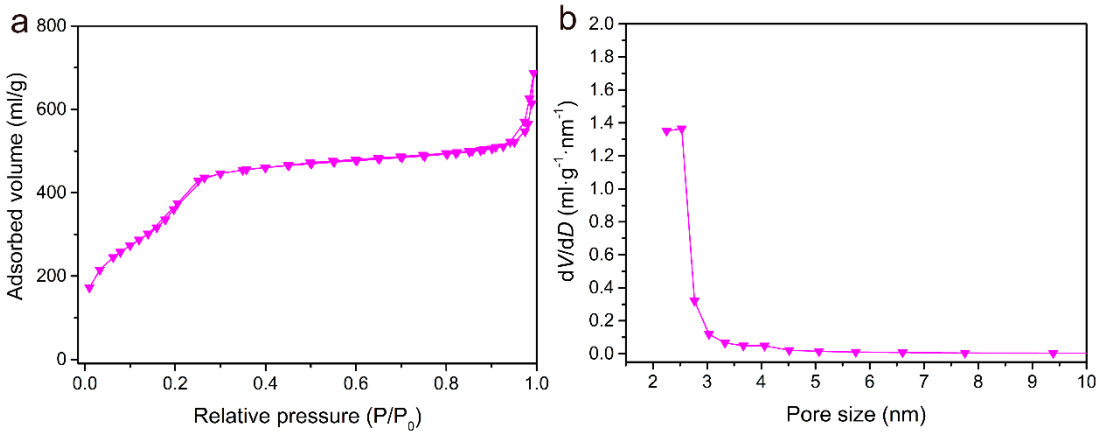

Figure S3. (**a**) N_2 adsorption-desorption isotherm curve; (**b**) BJH pore size distributions of mesoporous silica materials.

The N_2 adsorption-desorption isotherm of mesoporous silica materials had a typical type IV class according to the IUPAC classification, corresponded to mesoporous silica (Figure S3a).The BET surface area, pore volume and average pore diameter of these samples were 1499 m^2/g, 1.26 cm^3/g, and 2.8 nm according to the N_2 adsorption-desorption isotherms and pore size distribution curves of mesoporous silica materials (Figure S3).

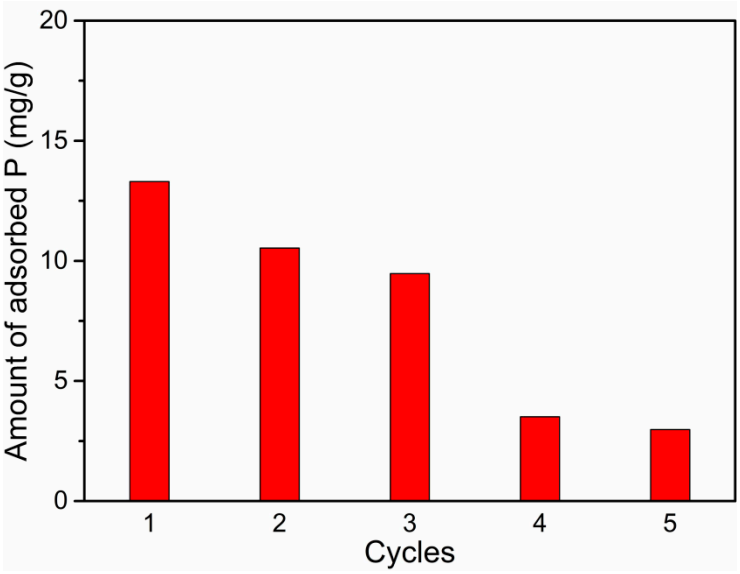

Figure S4. Regeneration of MALS-B under five consecutive adsorption-desorption cycles.

The regenerability of MALS-B under five consecutive adsorption-desorption cycles was assessed. And the corresponding result is shown in Figure S4. At the first regeneration, 79.2% of the phosphorus adsorption capacity could be realized in the regenerated MALS-B. After five consecutive cycles, the phosphorus adsorption capacity remained at approximately 22.4% of the initial value. Such a reduction could be attributed to thechemisorption of phosphate.

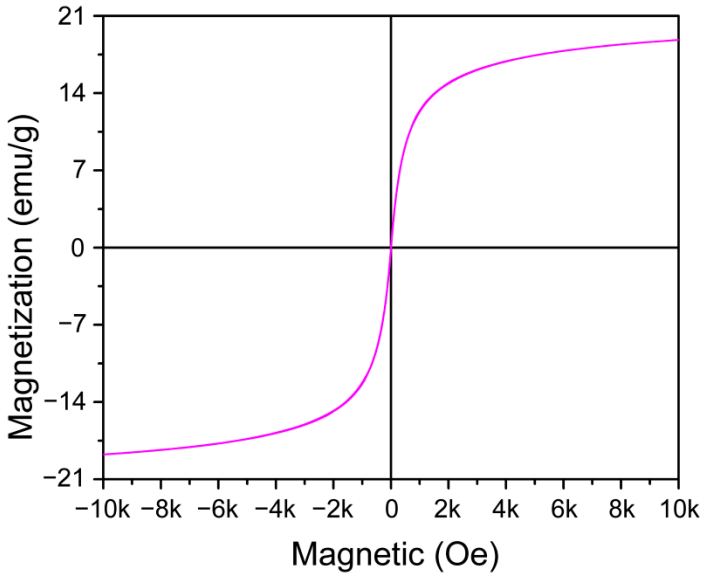

Figure S5. Magnetic hysteresis curve of MALS-B after phosphate adsorption.

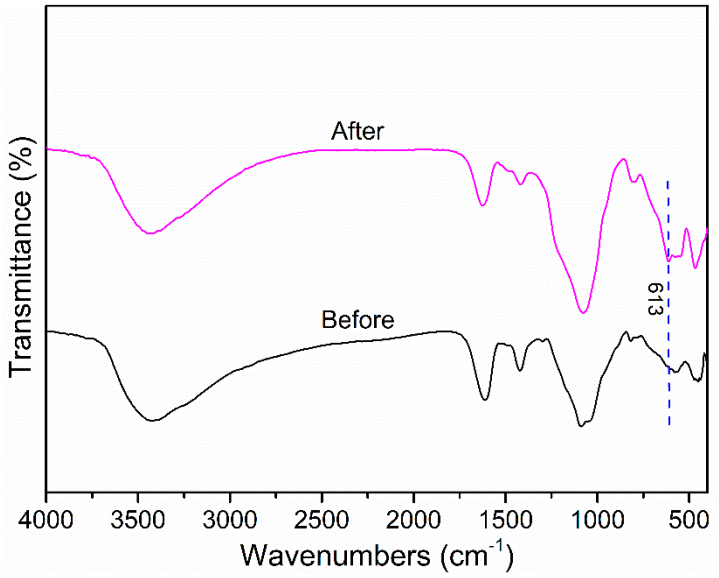

Figure S6. FTIR spectra of MALS-B before and after phosphate adsorption.